


 Cite this: *Nanoscale*, 2020, **12**, 16934

Synthesis of large gold nanoparticles with deformation twinings by one-step seeded growth with Cu(II)-mediated Ostwald ripening for determining nitrile and isonitrile groups†

 Chenshuo Wu,^a Hongpeng He,^a Yahui Song,^a Cuixia Bi,^a Lixiang Xing,^a Wei Du,^b Shenggang Li^c and Haibing Xia^{*a}

In this work, uniform and large gold nanoparticles (Au NPs) including quasi-spherical (QS) Au NPs with average diameters of 70 to 196 nm and trisoctahedral (TOH) Au NPs with average diameters of 140 to 195 nm were successfully synthesized by controlling the concentration of Cu²⁺ ions and the particle number of 3 nm Au-NP seeds, respectively, using a one-step seeded growth method with Cu²⁺-mediated Ostwald ripening. It is found that because of the concentration-dependent under-potential deposition of Cu²⁺ ions (Cu_{UPD}), 3 nm Au-NP seeds are firstly changed into Au NPs with a controlled QS- or TOH shape at the initial growth stage, followed by the conformal growth of Au atoms onto the initially formed Au NPs due to Cu²⁺-mediated Ostwald ripening, in which the extra Au atoms come from the dissolution of *in situ* Au nuclei by the unavoidable self-nucleation. Moreover, the as-prepared QS Au NPs with a rough surface exhibit a better SERS performance for physically adsorbed probes (crystal violet, CV) than the TOH Au NPs with sharp tips and with a comparable size. Furthermore, the as-prepared QS Au NPs can be used to distinguish nitrile and isonitrile groups by surface-enhanced Raman scattering (SERS) due to the presence of deformation twinings. Thus, the as-prepared QS Au NPs with a rough surface and deformation twinings can be further used as templates for the fabrication of bimetallic materials with multi-functionalities.

Received 23rd June 2020,

Accepted 10th July 2020

DOI: 10.1039/d0nr04733c

rsc.li/nanoscale

1. Introduction

Due to their unique localized surface plasmonic resonance (LSPR), gold nanoparticles (Au NPs) have been extensively studied for surface-enhanced Raman scattering (SERS) applications.^{1–6} In addition, their morphologies and sizes can heavily impact their SERS performance.^{3–6} Currently, the seeded growth method can readily achieve the synthesis of Au NPs with controlled morphology and a small size by modifying and adjusting the shape and the amount of the seeds, respect-

ively (Fig. 1a).^{7–11} In this method, the additional Au NPs as seeds can grow into uniformly large Au NPs. However, the occurrence of self-nucleation in the seeded growth method should be avoided; otherwise, the uniformity of the final products will be affected because the size and shape of the final product formed by the nuclei generated by self-nucleation are different from those formed by the additional Au NPs as seeds (Fig. 1c).^{7,12–16} For example, when monodispersed quasi-spherical (QS) Au NPs are prepared by a traditional one-step seeded growth method in the cetyltrimethylammonium chloride (CTAC) solution, their sizes are limited to 70 nm under optimized reaction conditions (Fig. 1a, b and S1, S2, ESI†). Moreover, when the average size of Au NPs is larger than 70 nm, self-nucleation is inevitable in the traditional one-step seeded growth method. Accordingly, poly-dispersed Au NPs are obtained due to co-existence of the byproducts formed by the Au nuclei and the main products formed by the additional Au-NP seeds (Fig. 1c and d). Thus, many researchers have investigated the adverse effect of self-nucleation in the traditional one-step seeded growth method used for synthesizing large NPs.^{16–20} To avoid self-nucleation, the multi-step seeded growth method was developed to prepare high quality large

^aState Key Laboratory of Crystal Materials, Shandong University, Jinan, 250100, P. R. China. E-mail: hbxia@sdu.edu.cn

^bSchool of Environment and Material Engineering, Yantai University, Yantai 264005, Shandong, China

^cCAS Key Laboratory of Low-Carbon Conversion Science and Engineering, Shanghai Advanced Research Institute, Chinese Academy of Sciences, 100 Haike Road, Shanghai 201210, China

†Electronic supplementary information (ESI) available: Additional TEM images of QS and TOH Au NPs; optical images of SERS substrates; extinction spectra of QS and TOH Au NPs; additional SERS spectra of CV probes; the calculation of EFs; extinction spectra of the reduction of 4-NP; Tables S1 to S4. See DOI: 10.1039/d0nr04733c

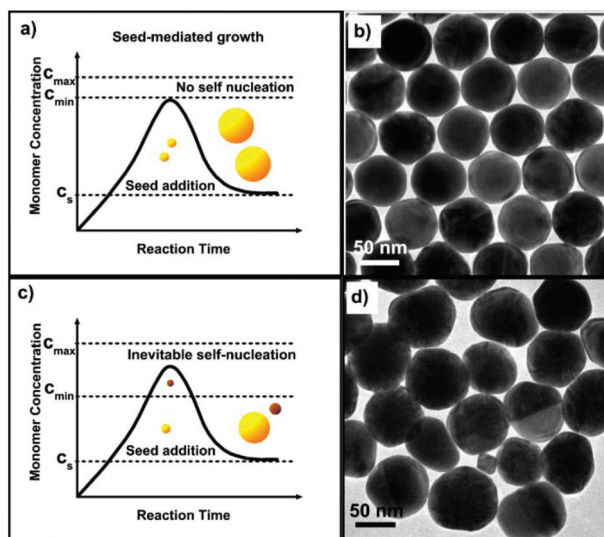


Fig. 1 Schematic representation of the formation process of Au NPs by a modified Lamer model (a and c) and their corresponding TEM images (b and d) in the one-step seeded growth method without (a and b) and with self-nucleation (c and d). The concentration of HAuCl₄ and ascorbic acid (AA) were fixed at 2.5 μM and 3.75 μM, respectively. The particle number of CTAC-capped Au-NP seeds used for the synthesis of Au NPs (b and d) was 1.56×10^{10} and 8.3×10^9 , respectively. Note that c_s is the saturation concentration of the monomer; and c_{\min} and c_{\max} are the minimum and maximum value of critical nucleation concentration, respectively.

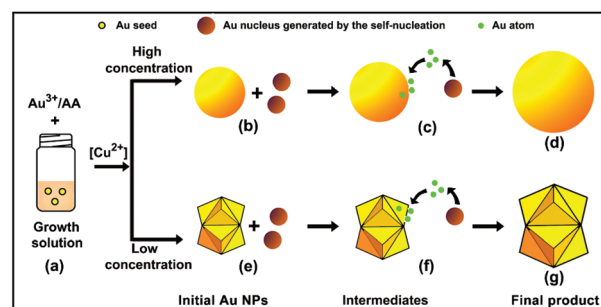
NPs with different shapes.^{7,21–23} For example, QS Au NPs with sizes of 70 to 150 nm were obtained by the three-step seeded growth method, in which 0.75 nm Au clusters and 10 nm and 46 nm Au NPs were used as the seeds.²² In addition, our group also reported the synthesis of {331}-faceted trisoctahedral (TOH) Au NPs with sizes of 60 to 255 nm by the multi-step seeded growth method.²³ However, the experimental operation of the multi-step seeded growth method is still too complex for researchers unfamiliar with material synthesis. Therefore, Au NPs can find many more applications if large Au NPs with various morphologies can be fabricated by the one-step seeded growth method.

At present, Ostwald ripening has been used to synthesize uniform NPs and nanostructured materials with multifunctionalities.^{24–28} For example, Yin *et al.* reported the synthesis of large octahedral Pd NPs (about 52 nm) by adding small Pd NPs (about 5 nm) as “sacrificial nanocrystals” (SNCs) into the solution containing the medium-sized octahedral Pd NPs (about 37 nm), in which these SNCs would dissolve into Pd atoms and further deposit onto the octahedral Pd NPs by Ostwald ripening with the assistance of formaldehyde.²⁸ Thus, it is necessary to introduce an extra reagent for conformal growth of the pre-formed NPs because the re-deposition of the dissolved atoms onto the pre-formed NPs is always uncontrollable during the Ostwald ripening process.

Meanwhile, it is known that the order of the under-potential deposition (UPD) of Cu²⁺ ions (Cu_{UPD}) onto the facets of Au NPs is (110) > (100) > (111).²⁹ Accordingly, the sequence of

Cu_{UPD} on the surface of Au NPs is concentration-dependent, that is, Cu_{UPD} mainly takes place on the (110) planes of Au NPs at a low concentration of Cu²⁺ ions. Moreover, at increasing concentration of Cu²⁺ ions, Cu_{UPD} would occur in the order the (100) and (111) planes of Au NPs. Therefore, the relative growth rate of the low-index planes of Au NPs can be impacted by introducing different concentrations of Cu²⁺ ions into the growth solution, which can result in the persistence or the disappearance of these low-index planes,^{30–32} and further determine the morphology of the final NPs. Inspired by these ideas, a one-step seeded growth method with Cu²⁺-mediated Ostwald ripening is proposed. In this method, when self-nucleation is inevitable during the synthesis of high quality large Au NPs, the introduction of Cu²⁺ ions into the growth solution can regulate 3 nm Au-NP seeds (Fig. S3, ESI[†]) into initial Au NPs with a controlled morphology at the initial growth stage (Scheme 1b and e) due to the concentration-dependent Cu_{UPD} effect. Meanwhile, the Au nuclei generated by the self-nucleation (brown particles in Scheme 1), instead of the further growth into Au NPs, would dissolve into Au atoms (green particles in Scheme 1) and further deposit onto the specific facets of the surfaces of the initial Au NPs with a controlled morphology due to the Cu²⁺-mediated Ostwald ripening, which would guarantee the conformal growth of the initial Au NPs with a controlled morphology (Scheme 1c and f). Eventually, the one-step seeded growth method with Cu²⁺-mediated Ostwald ripening can achieve the synthesis of large-sized Au NPs with high quality (Scheme 1d and g) by overcoming the adverse effect of self-nucleation on the size and shape of the final Au NPs.

Herein, firstly, uniform and large QS Au NPs with average diameters of 70 to 196 nm were successfully synthesized by controlling the concentration of Cu²⁺ ions and the particle number of 3 nm Au-NP seeds in the one-step seeded growth method with Cu²⁺-mediated Ostwald ripening. Next, the relationship between the size of the final QS Au NPs and the



Scheme 1 Schematic representation of the synthetic process of large-sized Au NPs with high quality by the one-step seeded growth method with Cu²⁺-mediated Ostwald ripening. (a) Addition of the solution of HAuCl₄, AA and Cu²⁺ ions into the glass vial; (b and e) the morphology of the initial Au NPs obtained at the high (b) and low (e) concentration of Cu²⁺ ions; (c and f) the conformal growth of quasi-spherical Au NP intermediates (c) and TOH Au NP intermediates (f) by the dissolution of Au nuclei into Au atoms and the further deposition due to Cu²⁺-mediated Ostwald ripening; and (d and g) the final large-sized, quasi-spherical Au NPs (d) and TOH-shaped Au NPs (g).

particle number of Au-NP seeds was discussed. Then, this method was extended to the synthesis of large {331}-faceted TOH Au NPs with average diameters of 140 to 195 nm by slightly changing the concentration of Cu^{2+} ions. Then, the concentration-dependent Cu_{UPD} effect and the role of Cu^{2+} -mediated Ostwald ripening in the formation of large Au NPs with a QS- or TOH-shape were investigated by TEM characterization of the changes in the morphology and size of the corresponding intermediates during the growth process. Then, the SERS performances of 70 nm QS Au NPs with deformation twinning and a rough surface as well as 70 nm TOH-shaped Au NPs with sharp tips on physically adsorbed probes (crystal violet, CV) were investigated. Finally, 70 nm QS Au NPs with deformation twinning and a rough surface were used for the determination of nitrile and isonitrile groups.

2. Experimental section

2.1 Materials and chemicals

Cetyltrimethylammonium chloride (CTAC, 99%), hydrogen tetrachloroaurate tetrahydrate ($\text{HAuCl}_4 \cdot 4\text{H}_2\text{O}$, 99%), sodium borohydride (NaBH_4 , 99%), L-ascorbic acid (AA, 99%), copper(II) nitrate trihydrate ($\text{Cu}(\text{NO}_3)_2 \cdot 3\text{H}_2\text{O}$, 99%), crystal violet (CV, $\text{C}_{25}\text{H}_{30}\text{N}_3\text{Cl}$), and 4-chlorobenzyl nitrile (4-CLBN, 98%) were purchased from Sinopharm Chemical Reagent Co. Ltd (Shanghai, China). Sodium tetrachloropalladate(II) (Na_2PdCl_4 , 99%), and 4-nitrophenol (4-NP, 99%) were purchased from Alfa Aesar (Shanghai, China). Reduced glutathione (GSH, 99%) and 2,6-dimethylphenyl isonitrile (2,6-DMPI, 97%) were purchased from Aladdin Co. Ltd (Shanghai, China) and Macklin Reagent (Shanghai, China), respectively. All chemicals were used as received without further treatment. The water used in all experiments was Milli-Q water (18 M Ω cm, Millipore). All glassware and stirring bars were thoroughly cleaned with aqua regia solutions (3 : 1 v/v HCl (37%) : HNO_3 (65%)) and washed with water before use. **Caution:** aqua regia solutions are dangerous and should be used with extreme care; never store these solutions in closed containers.

2.2 Preparation of 3 nm Au-NP seeds

The CTAC aqueous solution (0.1 M, 5 mL) and the aqueous solution of HAuCl_4 (10 mM, 0.125 mL) were sequentially added into a 10 mL glass vial under stirring at room temperature. Next, a freshly prepared ice-cold NaBH_4 solution (10 mM, 0.30 mL) was quickly injected into the CTAC- HAuCl_4 pre-mixture under vigorous stirring. Then, the resulting solution was stirred for at least 2 min for the complete decomposition of excess NaBH_4 . Finally, the glass vial containing 3 nm Au-NP seeds (Fig. S3, ESI[†]) was kept in a thermostatic water bath at 28 °C and used within 2–5 h after the preparation. Note that the resulting solution of 3 nm Au-NP seeds was diluted from 10 to 10 000 times before use.

2.3 Preparation of large-sized, QS- and TOH-shaped Au NPs

The procedure for the synthesis of QS Au NPs is as follows. Typically, the aqueous solutions of CTAC (50 mM, 5.0 mL),

Table 1 Summarized data of particle numbers of 3 nm Au-NP seeds (N_{seed}), the real diameters, calculated diameters, size deviations, and ellipticities of the as-prepared QS Au NPs obtained via our one-step seeded growth method with Cu^{2+} -mediated ripening, the measured and calculated center positions of their SPR peaks, and the figure numbers of the corresponding TEM images of the as-prepared QS Au NPs. The particle number concentration of 3 nm Au-NP seeds in the solution is about $1.04 \times 10^{11} \mu\text{L}^{-1}$. The concentration of HAuCl_4 in the reaction media is fixed at 2.5 μM

$N_{\text{seed}} [10^9]^a$	15.6	8.3	4.2	2.1	1.04	0.52
Real diameter [nm]	70	87	106	135	157	196
Calculated diameter [nm]	74	93	113	142	160	206
Standard Deviation [%] ^b	2.6	3.0	3.3	3.7	5.3	4.1
Ellipticity ^c	1.04	1.05	1.04	1.05	1.06	1.04
Exp. ^d						
Dipo. ^f [nm]	548	562	580	605	646	700
Quadru. ^g [nm]	None ^h	None	None	527	547	558
Mie ^e						
Dipo. [nm]	545	567	577	616	666	738
Quadru. [nm]	None	None	None	525	546	556
Sample image	2a	2b	2c	2d	2e	2f

^a The particle number of 3 nm Au-NP seeds in the growth solution.

^b Standard deviations of the diameters of the as-prepared QS Au NPs were calculated on the basis of the statistical results of at least 100 particles.

^c Ellipticity is estimated as the ratio of the major to minor axes. ^d The center positions of their SPR peaks measured by UV-vis spectroscopy. ^e The center positions of their SPR peaks calculated by using Mie theory. ^f Abbreviations of dipolar mode (nm). ^g Abbreviations of quadrupolar mode (nm). ^h None indicates that the corresponding SPR peaks are beyond the test wavelength range (300–1000 nm).

HAuCl_4 (10 mM, 0.25 mL), $\text{Cu}(\text{NO}_3)_2$ (10 mM, 0.2 mL), and AA (0.1 M, 50 μL) were sequentially added into a 10 mL glass vial under stirring at room temperature before the addition of 3 nm Au-NP seeds (0.15 μL , 1.56×10^{10}). The resulting mixture was then placed in a thermostatic water bath at 28 °C for the aging of 12 h. Finally, 70 nm QS Au NPs were obtained with the aid of centrifugation to remove the excess reactants. Accordingly, QS Au NPs with average diameters of 87, 106, 135, 157, and 196 nm were synthesized by varying the volumes of 3 nm Au-NP seeds from 0.08 to 0.04, 0.02, 0.01, and 0.005 μL . The corresponding particle numbers of 3 nm Au-NP seeds are 8.3×10^9 , 4.2×10^9 , 2.1×10^9 , 1.04×10^9 , and 5.2×10^8 , respectively (listed in Table 1).

The procedure for the synthesis of large-sized TOH Au NPs is the same as that of QS Au NPs, except the concentration of $\text{Cu}(\text{NO}_3)_2$ (1 mM, 40 μL). Accordingly, TOH Au NPs with an average diameter of 140 and 195 nm were synthesized by varying the volumes of 3 nm Au-NP seeds: 0.02 and 0.005 μL , respectively. The corresponding particle numbers of 3 nm Au-NP seeds are 2.1×10^9 and 5.2×10^8 , respectively.

The extinction spectra of the as-prepared Au NPs were recorded by using Mie plot software accordingly.

2.4 Preparation of samples for SERS

In a typical procedure, the glass substrates were cleaned by separately immersing in aqua regia and piranha solution (sulphuric acid/ $\text{H}_2\text{O}_2 = 7 : 3$) for 20 min before use, followed by thorough rinse with water, and drying with N_2 gas. After the treatment, 15 μL of the aqueous suspensions of 70 nm QS- or

TOH-shaped Au NPs were dropped onto the glass substrates, followed by drying at room temperature. The samples used for SERS experiments were prepared by immersing the glass substrates in the 10 mL ethanol solution containing the corresponding probes (CV, 4-CLBN, or 2,6-DMPI) for 4 h. Then, the glass substrates were taken out, thoroughly rinsed with ethanol and dried with N₂ gas. All samples were immediately used for SERS measurements after their preparation. The final concentrations of CV, 4-CLBN, and 2,6-DMPI used in our work were 10⁻³–10⁻⁹ M, 10⁻⁵ M, and 10⁻⁵ M, respectively.

2.5 Characterization

Transmission electron microscopy (TEM) and high-resolution TEM (HRTEM) images were obtained with a JEOL (JEM 2100F) transmission electron microscope operating at an acceleration voltage of 200 kV. The extinction spectra of the as-prepared Au NPs were recorded using a Cary 50 spectrophotometer. The SERS measurements were conducted using a Renishaw inVia Reflex Raman spectrometer with a 633 nm laser at room temperature.

3. Results and discussion

3.1 Preparation and characterization of large QS Au NPs

In our one-step seeded growth method with Cu²⁺-mediated Ostwald ripening for the synthesis of QS Au NPs, the concentration of Cu²⁺ ions is essential for obtaining uniformity in shape and size (Fig. S4, ESI[†]). For instance, when the concentration of Cu²⁺ ions is about 2 μM, monodispersed QS Au NPs with an average diameter of 70 nm were fabricated (Fig. S4c, ESI[†]). Fig. 2 shows TEM images of QS Au NPs of different sizes

synthesized by adjusting the particle number of 3 nm QS Au-NP seeds at fixed concentrations of Cu²⁺ ions (2.0 μM), Au precursor (2.5 μM) and AA (5.0 μM). The detailed procedures are listed in Table S1 (ESI[†]). It can be clearly seen that the average diameter of the as-prepared Au NPs increases from 70 nm to 87, 106, 135, 157 and 196 nm, when the particle number of Au-NP seeds (N_{seed}) decreases from 1.56×10^{10} to 8.3×10^9 , 4.2×10^9 , 2.1×10^9 , 1.04×10^9 , and 5.2×10^8 , respectively (Fig. 2a–f). Moreover, the standard deviations and the ellipticities of all the as-prepared Au NPs are relatively low and close to 1, respectively, which are calculated to be less than 5.3% and 1.06, respectively (Table 1).

These results indicate that the as-prepared Au NPs have a fairly narrow size distribution and a perfect quasi-spherical shape, respectively. In addition, the adverse effect of the Au nuclei generated by the unavoidable self-nucleation on the size and shape of the final Au NPs is overcome. Although the average diameters of all the as-prepared Au NPs are larger than 70 nm, they are colloiddally stable in water and their quasi-spherical shapes remain hardly changed for at least 1 month. Note that the as-prepared Au NPs easily sediment after a certain period of time during the storage, although they can be readily re-dispersed *via* hand shaking or gentle sonication without aggregation. Furthermore, the magnified TEM image of an individual QS Au NP with an average diameter of 70 nm was selected to show their typically rough surfaces (Fig. 2g). In addition, rich deformation twinings are observed by close views of their surfaces, as shown in the HRTEM image (Fig. 2h). The formation of rough surfaces and rich deformation twinings in the as-prepared Au NPs are attributed to the introduction of Cu²⁺ ions.^{32–34} Note that based on the results of the XPS and the HAADF-STEM-EDS mapping in our

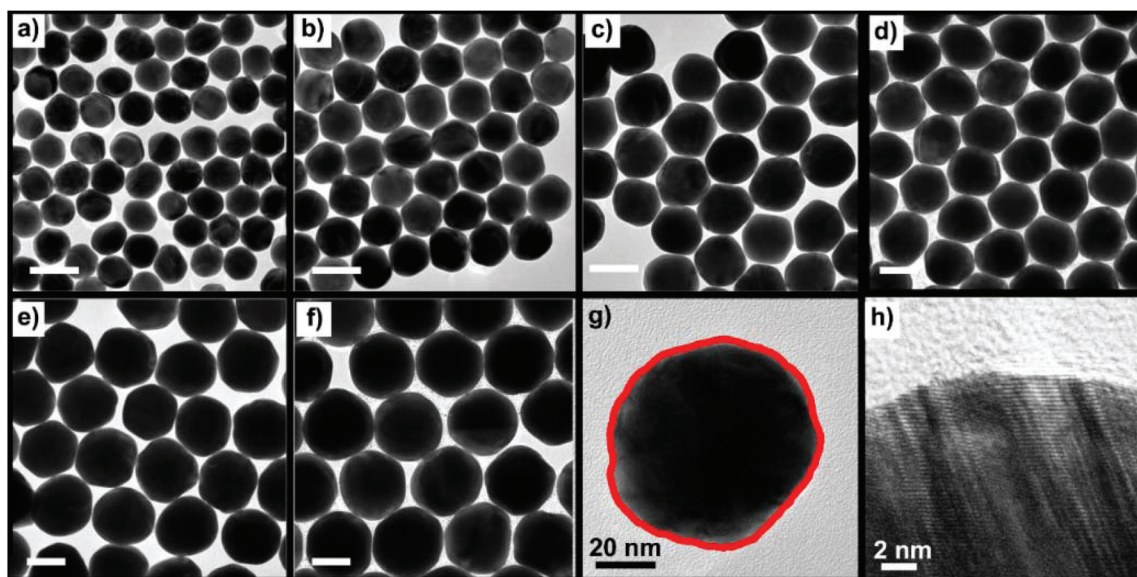


Fig. 2 Low-magnification TEM images (a to f) of the as-prepared Au NPs with various sizes: 70 nm (a), 87 nm (b), 106 nm (c), 135 nm (d), 157 nm (e), and 196 nm (f). High-magnification TEM image (g) of one individual QS Au NP with an average diameter of 70 nm and high resolution (HR) TEM image (h) of its typically rough surface. The scale bar in (a to f) is 100 nm. The concentration of Cu²⁺ ions, HAuCl₄ and AA is fixed at 2.0 μM, 2.5 μM and 5.0 μM, respectively. And the particle number of Au-NP seeds is listed in Table 1.

recent work,³³ the content of elemental Cu in the final QS Au NPs can be ignored. Therefore, Cu²⁺ ions just regulate the growth kinetics of the Au NPs but do not exist in the final Au NPs.^{30,33,35}

Fig. 3a shows the extinction spectra of the as-prepared QS Au NPs (in Fig. 2) and the photographs of their corresponding aqueous dispersions. It is found that by increasing their average diameters, the center positions of the dipolar surface plasmon resonance (SPR) peaks of the as-prepared QS Au NPs gradually red-shift to a longer wavelength, which is consistent with their size-dependent optical properties. For instance, when the average diameter increases from 70 to 106 nm, the center position of their dipolar SPR peaks gradually red shifts from 548 to 580 nm accordingly. In addition, the as-prepared QS Au NPs exhibit rather symmetric dipolar SPR peaks with a narrow half-width (Fig. 3a and Table 1). The results indicate that the as-prepared Au NPs with diameters of 70 to 106 nm are monodispersed and bear a nearly perfect spherical shape. Note that these Au NPs with average diameters smaller than 106 nm exhibit only one main SPR peak in their corresponding extinction spectra. It is also found that when further increasing their diameters, the dipolar SPR peaks of the as-prepared QS Au NPs are broadened and their center position is still red-shifted. In addition, the shoulder SPR peaks appear (the quadrupolar SPR peak) and gradually become pronounced. For instance, when the average diameter of QS Au NPs increases from 135 to 157 nm, their main dipolar SPR peaks start to broaden and the center positions of their main dipolar SPR peaks and quadrupolar SPR bands red shift from 605 to 646 nm and from 527 to 547 nm, respectively (Fig. 3a and Table 1). Note that Au NPs with an average diameter above 135 nm have noticeable quadrupolar SPR peaks.

The broadening of the dipolar SPR peaks and the appearance of quadrupolar SPR peaks are possibly due to the increasing radiative losses of the QS Au NPs with larger sizes and the phase retardation effect, respectively.^{36,37} When the average diameter of the as-prepared QS Au NPs is above 196 nm, the quadrupolar SPR peak evolves as the main SPR peak, while the

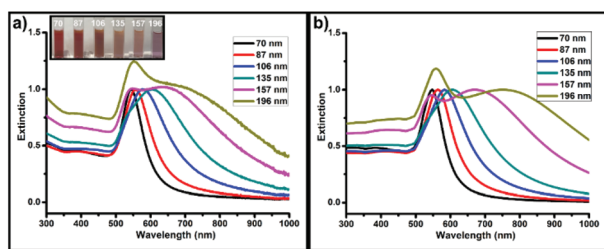


Fig. 3 (a) Extinction spectra of differently sized QS Au NPs obtained by our one-step seeded growth method with Cu²⁺-mediated ripening. The concentration of Cu²⁺ ions, HAuCl₄ and AA is fixed at 2.0 μM, 2.5 μM and 5.0 μM, respectively. The N_{seed} values used are listed in Table 1. The inset in (a) is the photographs of the aqueous dispersions of the corresponding QS Au NPs. (b) Extinction spectra of Au NPs with a perfect spherical shape calculated on the basis of Mie theory with the same sizes and standard deviation rates as the corresponding QS Au NPs obtained experimentally.

center positions of their dipolar SPR peak and quadrupolar SPR peak are located at about 700 nm and 558 nm, respectively. The continuous red-shift in the center positions of the SPR peaks of the as-prepared QS Au NPs with increasing NP diameters is also clearly reflected in the variation of the color of their aqueous dispersions (inset in Fig. 3a). According to their average diameters and the standard size deviations, the extinction spectra of all the as-prepared Au NPs are calculated by the Mie theory and shown in Fig. 3b.³⁸ By contrast, the experimental extinction spectra are consistent with the ones calculated from the Mie theory (Fig. 3 and Table 1).

Since the model used for the calculations by the Mie theory assumes that Au NPs have a perfectly spherical shape, the good match between the experimental and theoretical spectra indicates that the as-prepared Au NPs have a good quasi-spherical shape and have a narrow size distribution^{38,39} (as shown in the TEM images in Fig. 2). In the traditional seeded growth method, if all of the gold precursors used in the growth solution are consumed by deposition onto the additional Au-NP seeds during the seeded growth, and the shape of the final Au NPs is spherical, the average diameter of the final Au NPs can be quantitatively estimated using eqn (1):^{9,11,40}

$$r_{\text{Au NP}}^3 = r_{\text{seed}}^3 + \frac{3}{4\pi\rho_{\text{Au}}} \frac{m_{\text{Au}}}{N_{\text{seed}}} \quad (1)$$

where $r_{\text{Au NP}}$ is the theoretical radius of the as-prepared Au NPs; r_{seed} is the radius of the additional Au-NP seeds; m_{Au} is the mass of Au obtained *via* the reduction of HAuCl₄ in the growth solution; ρ_{Au} is the density of bulk Au. The number of the as-prepared Au NPs is assumed to be equal to N_{seed} . In our one-step seeded growth method with Cu²⁺-mediated Ostwald ripening, the Au nuclei generated by the unavoidable self-nucleation can also deposit onto the additional Au-NP seeds by the dissolution into Au atoms. Thus, the average diameter of the as-prepared Au NPs should also follow eqn (1). As expected, the calculated average diameters of the as-prepared Au NPs are fairly comparable to those experimentally obtained with a discrepancy of less than 10 nm (Table 1). In addition, the relationship between the experimentally measured radius of the as-prepared Au NPs ($r_{\text{Au NP}}$) and the negative cube root of the particle number of the additional Au-NP seeds ($N_{\text{seed}}^{-1/3}$) is indeed well fitted by eqn (1) with $R^2 = 0.996$ (Fig. 4). The results indicate that the Au nuclei generated by self-nucleation are indeed dissolved into Au atoms and further deposited onto the additional Au-NP seeds, instead of growing into the byproducts.

Moreover, the established relationship between the $r_{\text{Au NP}}$ and the N_{seed} in Fig. 4 also suggests that in our one-step seeded growth method with Cu²⁺-mediated Ostwald ripening, the diameters of the final Au NPs can also be precisely regulated by the number of the additional Au-NP seeds at the fixed HAuCl₄ precursors as predicted by eqn (1).

3.2 Preparation and characterization of large-sized TOH Au NPs

In our previous work and others,^{20,23,41} {331}-faceted TOH Au NPs with average diameters larger than 120 nm have to be syn-

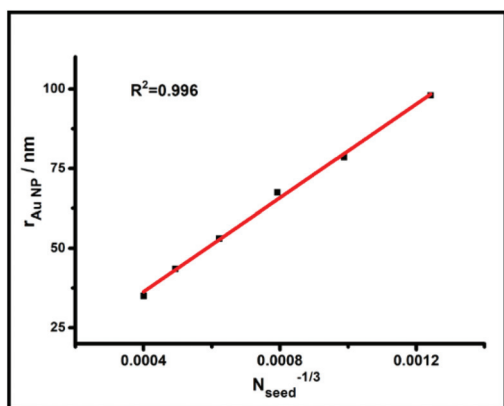


Fig. 4 Linear relationship between the radius of the as-prepared quasi-spherical Au NPs ($r_{\text{Au NP}}$) and the particle number of the Au-NP seeds (N_{seed}) in the growth solution.

thesized by the multi-step seeded growth method, since the yield of large-sized $\{331\}$ -faceted TOH Au NPs prepared by the one-step seeded growth method is rather low, accompanied by a high ratio of byproducts (Fig. S5, ESI†). In view of the success in the preparation of large QS Au NPs, our one-step seeded growth method with Cu^{2+} -mediated Ostwald ripening is also attempted for preparing large $\{331\}$ -faceted TOH Au NPs, based on our previous work.²³ Note that the optimal concentration of Cu^{2+} ions for the preparation of TOH Au NPs is $0.04 \mu\text{M}$ (Fig. S6, ESI†), instead of $2 \mu\text{M}$, possibly due to the concentration-dependent Cu_{UPD} effect. As expected, monodispersed TOH Au NPs with average diameters of 140 nm and 195 nm with a narrow distribution in size and shape are shown in Fig. 5a and d, respectively. Moreover, by measuring

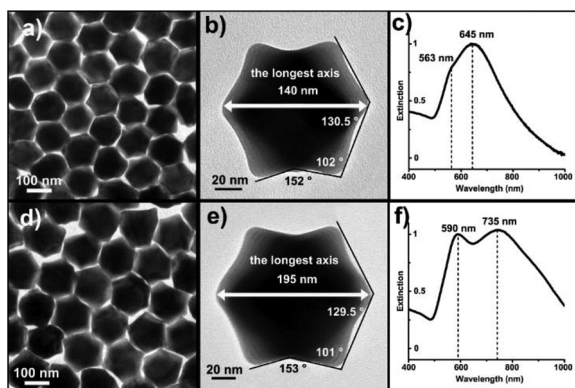


Fig. 5 Low (a and d), high magnification (b and e) TEM images and the corresponding extinction spectra (c and f) of $\{331\}$ -faceted TOH NPs with average diameters of 140 nm (a–c) and 195 nm (d–f) obtained under different particle numbers of 3 nm Au-NP seeds: 2.1×10^9 (a), 5.2×10^8 (d). The characteristic angles are labeled in high magnification TEM images (b and e) of the representatively individual TOH Au NP, viewed along the $\langle 110 \rangle$ direction. Note that the average diameter of TOH-shaped NPs is defined as the length of the longest axis viewed along the $\langle 110 \rangle$ direction in general. The concentrations of Cu^{2+} ions, HAuCl_4 , and AA were fixed at $0.04 \mu\text{M}$, $2.5 \mu\text{M}$ and $5 \mu\text{M}$, respectively.

their projection angles viewed along the $\langle 110 \rangle$ direction,^{23,41–43} the α , β , and γ angles of the as-prepared individual Au TOH NP with average diameters of 140 nm (130.5° , 102° , 152°) and 195 nm (129.5° , 101° , 153°) (Fig. 5b and e) are in good agreement with the Miller indices of NPs bound by $\{331\}$ facets (Table S3, ESI†). And one geometric model of a single TOH NP viewed along the $\langle 110 \rangle$ direction is illustrated in Fig. S7 (ESI†) for better understanding. Thus, large $\{331\}$ -faceted TOH Au NPs are also successfully synthesized by our one-step seeded growth method with Cu^{2+} -mediated Ostwald ripening. Furthermore, the extinction spectra of the as-prepared TOH Au NPs in this work are similar to those with the same size in our previous work (Fig. S8, ESI†).²³ For instance, the as-prepared 140 nm TOH Au NPs show a nearly symmetric dipolar SPR peak centered at about 645 nm with a weak quadrupolar SPR peak at about 563 nm (Fig. 5c). Moreover, 195 nm TOH Au NPs exhibit a dipolar SPR peak centered at 735 nm and an obvious quadrupolar SPR peak centered at 590 nm due to the phase retardation effect (Fig. 5f).^{23,37} Furthermore, with the increasing NP size, their main peaks (dipolar SPR) would red-shift and broaden, accompanied by the appearance of the obvious shoulder peaks.

3.3 Roles of $\text{Cu}(\text{u})$ ions in the synthesis of large Au NPs

To understand the role of Cu^{2+} ions in the synthesis of uniformly large Au NPs, a series of intermediate Au NPs including irregular Au NPs (Fig. 6A), TOH Au NPs (Fig. 6B) and QS Au NPs (Fig. 6C) formed at different reaction times were taken out for TEM characterization. Note that all reaction conditions are the same except for the concentration of Cu^{2+} ions. As shown in Fig. 6A, in the absence of Cu^{2+} ions, uniformly large Au NPs cannot be obtained by the traditional one-step seeded growth method due to the inevitable self-nucleation. In addition, due to the co-existence of additional Au-NP seeds and Au nuclei

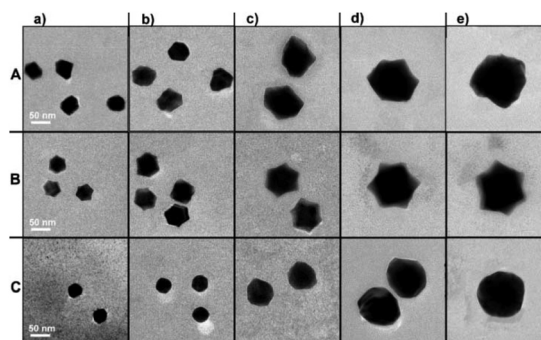


Fig. 6 TEM images of a series of the intermediates of irregular Au NPs (A), TOH Au NPs (B) and QS Au NPs (C), which were taken out at different reaction times: 60 s (a), 120 s (b), 240 s (c), 10 min (d), and 12 h (e). The procedures for the synthesis of three types of Au NPs (A, B and C) were the same except the concentrations of Cu^{2+} ions: $0 \mu\text{M}$ (A), $0.04 \mu\text{M}$ (B), and $2 \mu\text{M}$ (C). The concentrations of HAuCl_4 and AA were $2.5 \mu\text{M}$ and $5 \mu\text{M}$, respectively. The particle number of 3 nm Au-NP seeds was 2.1×10^9 . Note that the solution containing the intermediates was added into the freshly prepared glutathione (GSH) solution to limit their further growth.^{23,44}

generated by self-nucleation, the distribution in size and shape of the initial Au NPs are broad in the initial growth stage (Fig. 6A-a), possibly due to the missing regulation in the growth rate of facets on the surface of Au-NP seeds by the Cu_{UPD} effect. With the growth time increasing from 120 s to 240 s, and 10 min, the average size of the intermediates of large irregular Au NPs gradually increases from 50 to 100 and 130 nm, respectively (Fig. 6A-b, A-c, and A-d). However, the non-uniformity in shape and size of the intermediates and the final NPs remain during the entire growth period (Fig. 6A). In addition, there is hardly any Au nucleus (smaller than 5 nm) in the solution on the basis of TEM results. The results indicate that both additional Au-NP seeds and Au nuclei generated by self-nucleation grow into the final NPs without the Cu_{UPD} effect and Cu^{2+} -mediated Ostwald ripening, which result in the non-uniformity in the size and shape of Au NPs prepared in the absence of Cu^{2+} ions.

When an appropriate low concentration of Cu^{2+} ions is introduced into the growth solution, the Cu atoms would only deposit on the (110) facets of the Au-NP seeds. Accordingly, these (110) facets would steadily grow because of the Cu_{UPD} effect, instead of the rapid disappearance. Since the (111) facets are the most stable among them, Au (100) facets would grow rapidly and disappear eventually due to insufficient Cu^{2+} ions adsorbed on them. Therefore, 3 nm Au-NP seeds would grow into monodispersed, initial TOH Au NPs enclosed with (110) and (111) facets in the initial growth stage (Fig. 6B-a and Scheme 1e). However, when an appropriate high concentration of Cu^{2+} ions is introduced into the growth solution, the Cu atoms would be able to deposit simultaneously on the (110) and (100) facets of the Au-NP seeds at least. Under this situation, the (110) facets would rapidly disappear, while the (100) facets would steadily grow and be well maintained together with the most stable (111) facets. Therefore, at the initial growth stage, 3 nm Au-NP seeds would grow into monodispersed initial QS Au NPs enclosed with (100) and (111) facets (Fig. 6C-a and Scheme 1b).

In the presence of any concentration of Cu^{2+} ions, Au nuclei generated by self-nucleation can be observed and their amount gradually decreases with increasing growth time (Fig. S9, ESI[†]). The results indicate that Au nuclei would dissolve into Au atoms and further grow onto the pre-formed QS- or TOH Au NPs, instead of further growth into bigger Au NPs at the subsequent growth stage. With the assistance of the Cu_{UPD} effect, these Au atoms from the dissolution of Au nuclei can selectively grow onto the pre-formed QS- or TOH Au NPs. Therefore, Ostwald ripening in the presence of Cu^{2+} ions, called Cu^{2+} -mediated Ostwald ripening, can achieve the conformal growth of the corresponding Au NPs (Fig. 6B-b, B-c, B-d, C-b, C-c, C-d and Scheme 1f, c). Eventually, large Au NPs with a TOH- or QS-shape are successfully synthesized (Fig. 6B-e, C-e and Scheme 1g, d).

Briefly, the successful synthesis of large Au NPs with various shapes is realized by our one-step seeded growth method with Cu^{2+} -mediated Ostwald ripening, in which the morphology of the initial Au NPs can be controlled by the con-

centration-dependent Cu_{UPD} effect at the initial growth stage, followed by the dissolution of Au nuclei into Au atoms and the conformal growth of Au atoms onto the pre-formed initial Au NPs during the Cu^{2+} -mediated Ostwald ripening process.

3.4 SERS properties of QS Au NPs with rough surfaces

In SERS applications, Au NPs with a rough surface, sharp tips or both usually can exhibit excellent SERS performance due to the “hot-spot” effect.^{6,45–48} However, Au NPs with a rough surface and Au NPs with sharp tips: which have the better SERS performance for physically-adsorbed probes? Therefore, 70 nm QS Au NPs with a rough surface (Fig. 2a) and 70 nm TOH Au NPs with sharp tips (Fig. S10, ESI[†]) are separately used as SERS substrates to investigate their SERS performance on physically adsorbed probes, crystal violet (CV). To avoid the impact of other factors (*e.g.* the distance of adjacent NPs and the formation of NP aggregates) on the SERS intensity except the morphology, Au NPs (QS Au NPs or TOH Au NPs) should be discretely distributed on glass substrates without any aggregation.

After several rounds of attempts, the eligible SERS substrates were obtained by using a rather diluted dispersion of Au NPs (Fig. S11, ESI[†]). The Raman property and SERS performance of CV probes on the blank glass substrate and glass substrates coating with the corresponding Au NPs were investigated, respectively (Fig. S12–S14, ESI[†]). In addition, the enhanced factors (EFs) of 70 nm QS Au NPs with rough surfaces and 70 nm TOH Au NPs with sharp tips on different concentrations of CV probes were calculated accordingly (below Fig. S12, ESI[†]),^{23,49,50} on the basis of the intensity of the Raman band at 210 cm^{-1} of CV probes, which are plotted in Fig. 7. It is found that the EFs of CV probes on 70 nm QS Au NPs with rough surfaces are larger than and nearly equal to

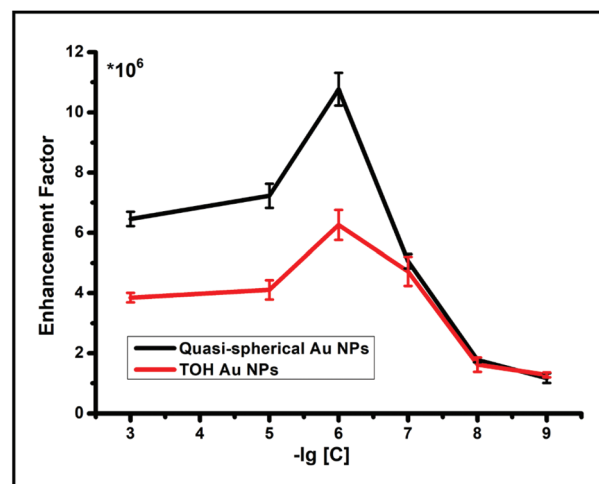


Fig. 7 Plots of the calculated enhanced factors (EFs) of different concentrations of CV probes on 70 nm QS Au NPs with a rough surface (black line) and 70 nm TOH Au NPs with sharp tips (red line) as SERS substrates vs minus logarithm of their corresponding concentrations ($-\lg [C]$).

those on 70 nm TOH Au NPs with sharp tips when the concentration of CV is in the range from 10^{-3} M to 10^{-7} M and from 10^{-7} M to 10^{-9} M, respectively (Fig. 7 and Table S4, ESI†).

The concentration-dependent SERS performance of 70 nm QS Au NPs with rough surfaces and 70 nm TOH Au NPs with sharp tips on CV probes is rather interesting. The results indicate that when they are at a high concentration (from 10^{-3} M to 10^{-7} M), physically adsorbed CV probes may mainly adsorb on the flat surfaces of TOH Au NPs with sharp tips and only a small fraction of them adsorb on their sharp tips (Fig. S15, ESI†). By contrast, all of the CV probes would adsorb on the surfaces of Au NPs with rough surfaces. Thus, the amount of CV probes on the flat surfaces of TOH Au NPs with sharp tips should be fewer than those on the surfaces of QS Au NPs with rough surfaces. Under this situation, the advantage of sharp tips as the “hot-spot” of TOH Au NPs with sharp tips is not fully utilized. Accordingly, the contribution of the sharp tips as the “hot-spot” to SERS enhancement would become minor and that of the flat surfaces of TOH Au NPs would dominate. Thus, the EFs of Au NPs with rough surfaces are larger than those of TOH Au NPs with sharp tips.

However, when they are at a low concentration (from 10^{-7} M to 10^{-9} M), CV probes may be fully adsorbed on the flat surfaces of TOH Au NPs with sharp tips and Au NPs with rough surfaces. Accordingly, the amount of CV probes on the flat surfaces of TOH Au NPs should be nearly equal to that on the surfaces of Au NPs with rough surfaces. Under this situation, the advantage of Au NPs with rough surfaces is not fully utilized. Thus, the contribution of TOH Au NPs to SERS enhancement mainly results from their flat surfaces, which is the same as that of Au NPs with rough surfaces. Accordingly, their EFs are the same. In brief, Au NPs with rough surfaces have a better SERS performance for physically adsorbed probes.

3.5 Determination of nitrile and isonitrile groups by SERS

The nitrile group (–CN) and isonitrile group (–NC), which are a pair of isomers, are still difficult to distinguish.^{51–53} It is known that whatever arrangement Au atoms on the surfaces of Au NPs have, the N atom of the –CN group always bonds to one Au atom, and the adsorption geometry is called “atop” configuration (Fig. S16a, ESI†).^{52,54,55} Accordingly, the nitrile group adsorbed on the SERS substrate composed of any type of Au NPs, and there is only one type of stretching frequency (ν_{CN} , ~ 2140 cm^{-1}) in its SERS spectrum⁵² due to the formation of the sole atop configuration. As expected, only one characteristic peak of the atop configuration (~ 2125 cm^{-1}) was observed in the SERS spectra of 4-chlorobenzyl nitrile (4-CLBN) (black and red curves in Fig. 8) obtained on the substrate coated with the single crystalline QS Au NPs (Au_s NPs) (Fig. S1, ESI†) or the as-prepared QS Au NPs with deformation twinning (Au_{dt} NPs) (Fig. 2).

However, when the isonitrile group binds the metal atoms, the adsorption geometry of the C atom on the surface of the metal NPs is highly dependent on the atom arrangement on their surfaces.^{53,56,57} For example, when the isonitrile group of 4-chlorophenyl isonitrile (CPI) binds the Pt (110) substrates,

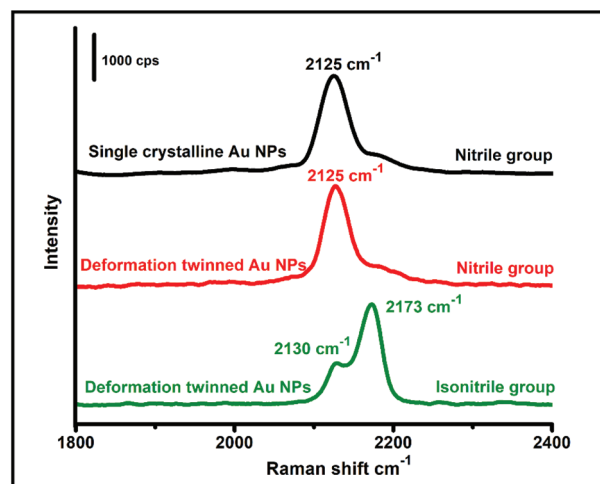


Fig. 8 SERS spectra of nitrile group adsorbed on the glass substrate coated with single crystalline QS Au NPs (black curve) and the glass substrate coated with QS Au NPs with deformation twinning (red curve), and isonitrile group adsorbed on the glass substrate coated with QS Au NPs with deformation twinning (green curve). The excitation laser wavelength for Raman measurements is 633 nm, and the laser power is 0.1 mW. The acquisition time is 10 s.

the C atom of the isonitrile group can bind one Pt atom by the atop configuration, and there is only one stretching frequency (ν_{NC} , ~ 2146 cm^{-1}) observed in the Raman spectrum of CPI.⁵³ When the isonitrile group of CPI binds the Pt {211} substrate, the C atom of the isonitrile group can bind one or three Pt atoms, thus resulting in the formation of atop or hollow configuration (Fig. S16b, ESI†). Accordingly, two types of stretching frequencies (ν_{NC} , ~ 2158 and ~ 1566 cm^{-1}) are observed in the SERS spectrum.⁵³ Therefore, on the basis of the difference in the adsorption geometry of the nitrile group and isonitrile group on Au NPs with a special bonding configuration, they may be determined by their SERS spectra. For instance, the SERS spectrum of 2,6-dimethylphenyl isonitrile (2,6-DMPI) obtained by using QS Au_{dt} NPs as the substrate shows two characteristic peaks, which belong to the atop configuration (~ 2173 cm^{-1}) and the hollow configuration (~ 2130 cm^{-1}), respectively (green curve in Fig. 8), in comparison with that of the nitrile group obtained by using QS Au_{dt} NPs as the substrate (red curve in Fig. 8). Due to the special adsorption geometry of the isonitrile group bonding to metal atoms in hollow configuration, the appearance of stretching frequency at about 2173 cm^{-1} can be used to distinguish nitrile and isonitrile groups.^{51,52} Therefore, the as-prepared QS Au NPs with deformation twinnings can be used as the SERS substrate to determine the nitrile and isonitrile groups by the SERS spectrum.

4. Conclusions

In summary, QS Au NPs with average diameters of 70 to 196 nm and TOH Au NPs with average diameters of 140 to 195 nm were successfully synthesized by our one-step seeded

growth method with Cu²⁺-mediated Ostwald ripening. It is found that the introduction of Cu²⁺ ions can avoid the adverse effect of self-nucleation in the traditional one-step seeded growth method. Moreover, the concentration-dependent Cu_{UPD} effect and the Cu²⁺-mediated Ostwald ripening process can achieve control in the morphology and the subsequent conformal growth of the initial Au NPs. Thus, our Cu²⁺-mediating Ostwald ripening method is beneficial for the simplification in the experimental operation.^{20,22,23,41} In addition, shape control of Au NPs can be achieved in one procedure by adjusting the concentration of Cu²⁺ ions. Furthermore, the as-prepared QS Au NPs with rough surfaces have a better SERS performance for physically adsorbed probes than the TOH Au NPs with sharp tips and with a comparable size. In addition, the as-prepared QS Au NPs used as the SERS substrate also can achieve distinguishing of the nitrile group and isonitrile group by SERS. Therefore, the as-prepared QS Au NPs can be further used as templates for the fabrication of bimetallic materials with multi-functionalities (say, hydrogenation catalysis (Fig. S17, ESI[†]), chemical catalysis, *in situ* SERS monitoring,⁵⁸ and so forth) due to the presence of rough surfaces and deformation twinnings.

Conflicts of interest

The authors declare no competing financial interest.

Acknowledgements

The authors are grateful to the financial support from the National Natural Science Foundation of China (21773142), Taishan Scholarship in Shandong Provinces (no. tsqn20161001), and Fundamental Research Funds of Shandong University.

Notes and references

- G. Yang, J. Nanda, B. Wang, G. Chen and D. T. Hallinan, *ACS Appl. Mater. Interfaces*, 2017, **9**, 13457–13470.
- W. Cao, L. Jiang, J. Hu, A. Wang, X. Li and Y. Lu, *ACS Appl. Mater. Interfaces*, 2018, **10**, 1297–1305.
- H. You, Y. Ji, L. Wang, S. Yang, Z. Yang, J. Fang, X. Song and B. Ding, *J. Mater. Chem.*, 2012, **22**, 1998–2006.
- L. Scarabelli, M. Coronado-Puchau, J. J. Giner-Casares, J. Langer and L. M. Liz-Marzán, *ACS Nano*, 2014, **8**, 5833–5842.
- J. Heo, D.-S. Kim, Z. H. Kim, Y. W. Lee, D. Kim, M. Kim, K. Kwon, H. J. Park, W. S. Yun and S. W. Han, *Chem. Commun.*, 2008, **46**, 6120–6122.
- K. Nehra, S. K. Pandian, C. Byram, S. S. B. Moram and V. R. Soma, *J. Phys. Chem. C*, 2019, **123**, 16210–16222.
- N. R. Jana, L. Gearheart and C. J. Murphy, *Chem. Mater.*, 2001, **13**, 2313–2322.
- A. Gole and C. J. Murphy, *Chem. Mater.*, 2004, **16**, 3633–3640.
- Y. Li, P. Zhang, J. Duan, S. Ai and H. Li, *CrystEngComm*, 2017, **19**, 318–324.
- X. Liu, H. Xu, H. Xia and D. Wang, *Langmuir*, 2012, **28**, 13720–13726.
- N. G. Bastús, J. Comenge and V. Puntes, *Langmuir*, 2011, **27**, 11098–11105.
- L.-C. Cheng, J.-H. Huang, H. M. Chen, T.-C. Lai, K.-Y. Yang, R.-S. Liu, M. Hsiao, C.-H. Chen, L.-J. Her and D. P. Tsai, *J. Mater. Chem.*, 2012, **22**, 2244–2253.
- A. Umar, J. Lee, J. Dey and S.-M. Choi, *Chem. Mater.*, 2016, **28**, 4962–4970.
- L. Chen, F. Ji, Y. Xu, L. He, Y. Mi, F. Bao, B. Sun, X. Zhang and Q. Zhang, *Nano Lett.*, 2014, **14**, 7201–7206.
- W. Niu, L. Zhang and G. Xu, *Nanoscale*, 2013, **5**, 3172–3181.
- C. Gao, J. Vuong, Q. Zhang, Y. Liu and Y. Yin, *Nanoscale*, 2012, **4**, 2875–2878.
- C. Gao, J. Goebel and Y. Yin, *J. Mater. Chem. C*, 2013, **1**, 3898–3909.
- Y. Huang, A. R. Ferhan, Y. Gao, A. Dandapat and D.-H. Kim, *Nanoscale*, 2014, **6**, 6496–6500.
- A. U. Khan, Z. Zhou, J. Krause and G. Liu, *Small*, 2017, **13**, 1701715.
- Y. Yu, Q. Zhang, X. Lu and J. Y. Lee, *J. Phys. Chem. C*, 2010, **114**, 11119–11126.
- A. Govender, W. Barnard, E. J. Olivier, R. P. Forbes, E. van Steen and J. H. Neethling, *Mater. Charact.*, 2016, **121**, 93–102.
- Y. Zheng, X. Zhong, Z. Li and Y. Xia, *Part. Part. Syst. Charact.*, 2014, **31**, 266–273.
- Y. Song, T. Miao, P. Zhang, C. Bi, H. Xia, D. Wang and X. Tao, *Nanoscale*, 2015, **7**, 8405–8415.
- Y. Chen, E. Johnson and X. Peng, *J. Am. Chem. Soc.*, 2007, **129**, 10937–10947.
- C. C. Yec and H. C. Zeng, *J. Mater. Chem. A*, 2014, **2**, 4843–4851.
- W. Duan, P. Zhang, Y. Xiahou, Y. Song, C. Bi, J. Zhan, W. Du, L. Huang, H. Möhwald and H. Xia, *ACS Appl. Mater. Interfaces*, 2018, **10**, 23081–23093.
- R. F. Ali and B. D. Gates, *Chem. Mater.*, 2018, **30**, 2028–2035.
- Z. Zhang, Z. Wang, S. He, C. Wang, M. Jin and Y. Yin, *Chem. Sci.*, 2015, **6**, 5197–5203.
- F. Möller, O. M. Magnussen and R. J. Behm, *Electrochim. Acta*, 1995, **40**, 1259–1265.
- L. Zhang, Q. Chen, Z. Jiang, Z. Xie and L. Zheng, *CrystEngComm*, 2015, **17**, 5556–5561.
- W. Liu, H. Zhang, T. Wen, J. Yan, S. Hou, X. Shi, Z. Hu, Y. Ji and X. Wu, *Langmuir*, 2014, **30**, 12376–12383.
- J. Sun, M. Guan, T. Shang, C. Gao, Z. Xu and J. Zhu, *Cryst. Growth Des.*, 2008, **8**, 906–910.
- C. Wu, H. Li, H. He, Y. Song, C. Bi, W. Du and H. Xia, *ACS Appl. Mater. Interfaces*, 2019, **11**, 46902–46911.
- E. Ye, K. Y. Win, H. R. Tan, M. Lin, C. P. Teng, A. Mlayah and M.-Y. Han, *J. Am. Chem. Soc.*, 2011, **133**, 8506–8509.
- L. Zhang, J. Zhang, Q. Kuang, S. Xie, Z. Jiang, Z. Xie and L. Zheng, *J. Am. Chem. Soc.*, 2011, **133**, 17114–17117.

- 36 J. Rodríguez-Fernández, J. Pérez-Juste, F. J. García de Abajo and L. M. Liz-Marzán, *Langmuir*, 2006, **22**, 7007–7010.
- 37 H. Wang and N. J. Halas, *Adv. Mater.*, 2008, **20**, 820–825.
- 38 L. Xing, Y. Xiahou, P. Zhang, W. Du and H. Xia, *ACS Appl. Mater. Interfaces*, 2019, **11**, 17637–17646.
- 39 P. Zhang, Y. Li, D. Wang and H. Xia, *Part. Part. Syst. Charact.*, 2016, **33**, 924–932.
- 40 W. Leng, P. Pati and P. J. Vikesland, *Environ. Sci.: Nano*, 2015, **2**, 440–453.
- 41 Y. Yu, Q. Zhang, B. Liu and J. Y. Lee, *J. Am. Chem. Soc.*, 2010, **132**, 18258–18265.
- 42 Y. Ding, Y. Gao, Z. L. Wang, N. Tian, Z.-Y. Zhou and S.-G. Sun, *Appl. Phys. Lett.*, 2007, **91**, 121901.
- 43 N. Tian, Z.-Y. Zhou and S.-G. Sun, *J. Phys. Chem. C*, 2008, **112**, 19801–19817.
- 44 X. Kou, S. Zhang, Z. Yang, C.-K. Tsung, G. D. Stucky, L. Sun, J. Wang and C. Yan, *J. Am. Chem. Soc.*, 2007, **129**, 6402–6404.
- 45 R. Zhang, B.-B. Xu, X.-Q. Liu, Y.-L. Zhang, Y. Xu, Q.-D. Chen and H.-B. Sun, *Chem. Commun.*, 2012, **48**, 5913–5915.
- 46 C. Qiu, Y. Bao, N. L. Netzer and C. Jiang, *J. Mater. Chem. A*, 2013, **1**, 8790–8797.
- 47 H. Liang, Z. Li, W. Wang, Y. Wu and H. Xu, *Adv. Mater.*, 2009, **21**, 4614–4618.
- 48 Y. Wang, K. Wang, B. Zou, T. Gao, X. Zhang, Z. Du and S. Zhou, *J. Mater. Chem. C*, 2013, **1**, 2441–2447.
- 49 Q. Zhang, N. Large and H. Wang, *ACS Appl. Mater. Interfaces*, 2014, **6**, 17255–17267.
- 50 S. L. Kleinman, B. Sharma, M. G. Blaber, A.-I. Henry, N. Valley, R. G. Freeman, M. J. Natan, G. C. Schatz and R. P. Van Duyne, *J. Am. Chem. Soc.*, 2013, **135**, 301–308.
- 51 J. Hu, N. Hoshi, K. Uosaki and K. Ikeda, *Nano Lett.*, 2015, **15**, 7982–7986.
- 52 A. I. Guttentag, T. Wächter, K. K. Barr, J. M. Abendroth, T.-B. Song, N. F. Sullivan, Y. Yang, D. L. Allara, M. Zharnikov and P. S. Weiss, *J. Phys. Chem. C*, 2016, **120**, 26736–26746.
- 53 J. Hu, M. Tanabe, J. Sato, K. Uosaki and K. Ikeda, *J. Am. Chem. Soc.*, 2014, **136**, 10299–10307.
- 54 A. Tadjeddine and A. Le Rille, *Electrochim. Acta*, 1999, **45**, 601–609.
- 55 A. Le Rille, A. Tadjeddine, W. Q. Zheng and A. Peremans, *Chem. Phys. Lett.*, 1997, **271**, 95–100.
- 56 E. López-Tobar, K. Hara, I. Izquierdo-Lorenzo and S. Sanchez-Cortes, *J. Phys. Chem. C*, 2015, **119**, 599–609.
- 57 Y. Sohn and J. M. White, *J. Phys. Chem. C*, 2008, **112**, 5006–5013.
- 58 Y. Song, C. Xiang, C. Bi, C. Wu, H. He, W. Du, L. Huang, H. Tian and H. Xia, *Nanoscale*, 2018, **10**, 22302–22311.